Journal of Materials Research 28 (13) 1724-1728 (2013)

Epitaxy in solid phase thin film reactions: Nucleation controlled growth of iron silicide nanostructures on Si(001)

György Molnár[a)]

Institute of Technical Physics and Materials Science, Research Centre for Natural Sciences, HAS, Budapest H-1525 P.O. Box. 49, Hungary

Abstract

A special type of epitaxial growth appears during solid phase thin film reactions, where the reaction product grows epitaxially on the substrate. Some metal silicide layers and nanostructures are known to develop such epitaxial structures. In this study iron silicide was used to study the effect of the growth mode on the epitaxial growth. Strain-induced, self-assembled iron silicide nanostructures were grown on Si(001) substrates by electron gun evaporation of 1.0 nm iron and subsequent annealing at 500-850°C for 60 minutes. The growth processes were checked by reflection high energy electron diffraction, and the formed structures were characterized by scanning electron microscopy and optical microscopy. The iron silicide nanostructures were oriented in square directions epitaxially fitting to the surface of Si(001). The shape and size of the nanostructures depended on the annealing temperature. In some cases the nanoparticles were arranged in circles. This might be the direct consequence of a nucleation controlled type transition of iron monosilicide to iron disilicide phase at nanoscale.

[a)] Address all correspondence to this author.

E-mail: molnar.gyorgy@ttk.mta.hu

Journal of Materials Research 28 (13) 1724-1728 (2013)

1. Introduction

The fabrication of artificial low dimensional structures is one of the most challenging research fields in the solid state technology. These nanoobjects are prepared by physical and chemical or by combined methods and they have attracted great interest, due to their scientific peculiarity and technical significance. Nanostructures are applied both in bulk and low dimensional materials for composite materials, energy production, catalysis, optoelectronics, nanomagnetic materials, and for biomedicine [1]. One of the most challenging methods of nanostructure production is the phenomenon of self-assembly, that has been applied in the case of compound and group IV semiconductors and a wide range of material and substrate combinations [2].

During self-assembly phenomena, the natural laws are used as instruments to produce the nanostructures. The strain induced self-assembled growth is a basic physical method for the preparation of nanostructures. In the case of thin film growth three basic modes may occur, depending on the surface and interface free energies: Layer by layer growth (Frank-van der Merwe type), island growth (Volmer-Weber type), several complete monolayers formation and subsequently three dimensional clusters growth on the top of the first monolayers (Stranski-Krastanov type) [3]. The Stranski-Krastanov growth occurs mainly during epitaxial growth of films on monocrystalline substrates, as a consequence of lattice distortions due to lattice mismatch. The general concept of domain matching epitaxy is applicable across the whole misfit scale [4]. During the growth of strained layers, the film is able to remain planar up to a critical thickness that can be calculated based on the misfit

between the strained layer and film according to the domain matching epitaxy model. Above a critical thickness, three dimensional, dislocation free islands may form [5].

A special type of epitaxial growth appears during solid phase thin film reactions, where the reaction product grows epitaxially on the substrate. Metal silicide layers and nanostructures are known to develop such kinds of epitaxial structures. The growth mode during the thin film reaction modifies the epitaxial growth. Sometimes, the Stranski-Krastanov type growth occurs during the growth of epitaxial metal silicide films and silicide nanostructures [6].

Silicide layers are fabricated mainly from a metallic thin film (which is generally polycrystalline) and from silicon substrate in conventional solid phase reaction. During the growth, different formation modes are observable. The most important type is the diffusion controlled growth kinetics. All diffusion controlled reactions have an initial stage under a certain thickness, where they exhibit reaction controlled growth kinetics [7]. The next category of growth kinetics is the nucleation controlled reaction, where the nucleation of the new silicide phase is so difficult that it dominates the process of the phase formation [8-9]. The nucleation controlled reactions generally take place suddenly, producing rough surface structures, sometimes in peculiar, circular configurations.

Semiconducting β-$FeSi_2$ is one of the possible materials for future Si based optoelectronic devices and new generation thin film solar cells, which have to use abundantly available, non toxic and environmentally friendly chemical elements [10]. Efforts have been made to fabricate iron silicide based photovoltaic devices, because β-$FeSi_2$ has 23% theoretical efficiency in solar cells, and both its layer and nanoparticle forms have potential applications in photovoltaic technology [11-17]. Terasawa and coworkers

proposed a composite β-$FeSi_2$/Si film for photovoltaic use, where iron silicide nanoparticles are embedded in silicon. In this case photocarriers are generated in the iron silicide particles, which have high photoabsorption coefficient, while carrier transport happens in silicon. This kind of material may result in a superior solar cell as a consequence of its high photoabsorption coefficient and high carrier mobility [18].

Basically, β-$FeSi_2$ is an indirect semiconductor but, due to lattice distortions in epitaxial configurations on a silicon substrate, it shows a direct band gap [19, 20]. During solid phase thin film reactions the following phases of the Fe-Si equilibrium phase diagram have been found on Si substrates [21-24]: The mostly Fe-rich iron silicide is Fe_3Si (DO_3 type), with a cubic lattice. Two types of iron monosilicides might be present in thin film form. The first monosilicide phase is ε-FeSi with cubic structure and the second phase is cesium-chloride type cubic FeSi. The iron disilicides might appear with three different crystal structures. The high temperature, metastable, tetragonal α-$FeSi_2$ phase might be present in thin film form on Si substrates. The cubic γ-$FeSi_2$ phase is also metastable. Finally, the stable β-$FeSi_2$ has orthorhombic structure. All of the above phases, including metastable ones, might be epitaxially stabilized on the surface of Si substrates [25].

The objective of the recent study is to prepare iron silicide nanostructures by conventional – (iron evaporation onto room temperature Si substrate and subsequent annealing) – method, and investigate the formation kinetics at nanoscale. The FeSi to $FeSi_2$ phase transformation is a nucleation controlled process in thin film reactions [26]. The question is whether the previous nucleation controlled phase transformation had any effect on the morphology of the iron disilicide nanostructures. Previously, the existence of iron

silicide nanostructures was demonstrated in the case of reactive deposition epitaxy method, where iron particles were evaporated onto heated Si substrates [27]. This research may result in new knowledge in morphology changes of iron silicides and, on the practical side, may help to prepare more effective environmentally friendly solar cells, and Si based optoelectronics.

2. Experimental

Pieces of (001) oriented Si (p-type, 12-20 Ωcm) wafers were used as substrates. Before loading the samples into the oil free evaporation chamber, the oxide was removed in diluted HF. After evacuation down to $1*10^{-7}$ Pa and prior to evaporation, Si wafers were annealed in situ for 5 min at 850°C. Iron ingots of 99.9% purity were used as the evaporation source using an electron gun, at an evaporation rate of 0.01-0.03 nm/s, at a pressure of $3*10^{-6}$ Pa. The film thickness was measured by a quartz microbalance. The temperatures were monitored by small heat-capacity Ni-NiCr thermocouples. The initial Fe thickness was 1.0 nm and the subsequent annealing temperatures varied between 500 and 850°C. The annealing time was 60 minutes for all samples. During evaporation the substrates were held at room temperature and the subsequent annealing was carried out in situ in the same vacuum chamber. Additionally, a thick sample was prepared with 30 nm iron thickness, which was annealed at 600°C for 5 minutes.

The phases and structures were characterized by reflection high energy electron diffraction (RHEED), scanning- electron microscopy (SEM), and optical microscopy.

3. Results and discussions

The sample preparation was checked by RHEED. In Fig. 1(a) can be seen the RHEED image taken from the cleaned and annealed Si(001) substrate, which shows sharp 2x1 reconstruction. Weak, so-called Kikuchi lines are seen in the image, indicating the high quality of the Si(001) surface. After iron evaporation, in the case of 1.0 nm deposited Fe, the lines of RHEED image, originating from the substrate, totally disappeared, indicating that the iron film has polycrystalline character. After 60 min annealing at 500ºC according to the RHEED image a new, reconstructed surface developed, showing the epitaxial character of the formed iron silicide (Fig. 1(b)). These lines are weak and diffuse as a consequence of the moderate quality of the surface, which was grown at relatively low temperature (500ºC). Higher temperature annealing produced sharper lines in the RHEED images. In Fig. 1(c) can be seen the RHEED image of 1 nm Fe annealed at 600°C for 60 minutes, and in Fig. 1(d) 1 nm Fe annealed at 850°C for 60 minutes.

SEM images of the annealing temperature dependent formation of iron silicide nanostructures are presented in Figs. 2(a-c). The nominal "film thickness" was 1.0 nm for each sample, and the heat treatments were carried out at (a) 500, (b) 600, and (c) 850°C for 60 minutes. As can be seen, all of the samples show aggregated iron silicide nanostructures, but at different scales. The size and the distribution of the islands depend on the temperature. The average dimension of the islands found was between 20 and 100 nm. The density of islands decreased with increasing temperature of annealing, while the size of the nanostructures increased. The average number of nanostructures/μm^2, and the average size of the objects are listed in Table I. for the three annealing temperatures. In the case of lower annealing temperature (500°C) the characteristic shapes of nanostructures were dome like

and randomly shaped. Higher temperature annealing yielded triangular, rectangular, and elongated iron silicide nanostructures, which appear in square directions to each other in the plane of the surface, oriented epitaxially to the Si(001) substrate.

The detailed transmission electron microscopy phase analysis of iron silicide nanostructures was presented in our previous paper [27]. Where, the nanostructures contain three different iron disilicide phases, i.e. orthorhombic β-$FeSi_2$, cubic γ-$FeSi_2$, and tetragonal α-$FeSi_2$. The epitaxy relationships, as deduced from the diffraction pattern are: (a) $[14\bar{2}]$ β-$FeSi_2$ // [001] Si, (b) [001] γ-$FeSi_2$ // [001] Si and [100] γ-$FeSi_2$ // [100] Si, (c) $[\bar{1}2\bar{1}]$ α-$FeSi_2$ // (001) Si and [111] α-$FeSi_2$ // $<111>$ Si and $[\bar{1}01]$ α-$FeSi_2$ // $<\bar{4}80>$ Si and $<110>$ α-$FeSi_2$ // (001) Si and c axis of α-$FeSi_2$ is 22° of the $<1\bar{1}0>$ Si direction [27]. The ratio of the phases depends on the time and temperature of the annealing.

This ordering is a direct consequence of Ostwald ripening phenomena, where the bigger islands grow further at the cost of the smaller ones. In post deposition conditions where no additional material is being deposited, Ostwald ripening is considered the primary coarsening mechanism for island growth [28]. The role of the Ostwald ripening is reinforced by the existence of depleted regions near the bigger objects.

SEM images of the sample annealed at 600°C for 60 minutes show interesting surface arrangements at lower magnification. On the surface of the sample, randomly distributed circles with 4-6 micrometer diameter are seen (Fig. 3(a)). With the enhancement of the magnification of the microscope ((Figs. 3(b), (c)), the inner structure of the circles is more visible. The contours of the circles consist of nanostructures, which are locally bigger than their neighbours, and around them there are depleted regions. The question arises what is

the reason for the above special geometric arrangement. To answer the above question an additional, thick iron silicide sample was prepared from 30 nm iron, which was annealed at 600°C for 5 minutes. The optical microscopy image taken from this sample is shown in Fig. 4. The surface shows dense, randomly distributed, mainly coalesced circular objects with about 20 μm diameter in the background. This geometry is typical for nucleation controlled type silicide solid phase reactions [9]. The FeSi to $FeSi_2$ phase transformation is a nucleation controlled process [26]. The nucleation controlled solid phase reactions produce rough surfaces as a consequence of the coalescence of growing nuclei from different spots. The question may arise, whether these circles refer the nucleation controlled character of the reaction, or are artifacts. If the circular objects would be artifacts of improper cleaning or any other surface effects, they should have the same size in different samples. But, in the case of 1 nm Fe their size is in the 4 μm range (Figs. 3(a-c)), and for 30 nm Fe films their size is around 20 μm (Fig. 4), and Ref. [26] shows ~50 μm size circular objects from 150 nm Fe film. The size of the objects correlates the initial Fe film thickness. That is why they are not a consequence of an accidental interface contamination, but caused by the nucleation controlled growth mode of iron disilicide.

Apparently, the only possible explanation of the circles displayed in the sample with nanostructures (Figs. 3(a-c)) is a nucleation controlled type phase formation at the nanoscale too. It is interesting that the nanoobjects inside and at the contours of the circles show the same orientation as the other ones outside. The simultaneous effect of nucleation controlled growth mode and epitaxial growth resulted a peculiar arrangement and morphology of the iron silicide nanostructures.

It is worth mentioning that the epitaxial growth in solid phase thin film reactions basically differs from conventional deposit-substrate epitaxy. The initially polycrystalline layer reacts with the substrate, and the reaction products may grow epitaxially on the substrate. During the growth, the original (average) interface is shifted towards the substrate, because some of the original substrate material has been consumed to grow the silicide layer. In fact, epitaxial silicides form within the substrate, not on the substrate. This phenomenon has no special consequences in conventional planar thin film geometry, but in the case of nanostructures it has a spectacular impact. Sometimes, the nanostructures are sunk into the substrate [29]. Nowadays, this kind of epitaxy is called endotaxy (oriented growth within a substrate) [30], but this is only a subcategory of epitaxy.

4. Conclusions

Iron silicide nanoislands were grown by conventional Fe evaporation and subsequent annealing on Si(001) substrate. The size distribution and shape of the formed islands depended on the annealing temperatures. In the case of lower annealing temperature the characteristic shapes of nanostructures were dome like and randomly shaped. Higher temperature annealing resulted in triangular, rectangular, and elongated iron silicide nanoobjects, which are oriented in square directions. In some cases the nanoparticles were arranged in circles. This might be the direct consequence of a nucleation controlled type of local transition of iron monosilicide to the iron disilicide phase at nanoscale.

Acknowledgements

The author thanks Zofia Vertesy for SEM images. The support of OTKA Grant No. 81998 is acknowledged.

Journal of Materials Research 28 (13) 1724-1728 (2013)

References

1. C.P. Bergman, and M. Jung de Andrade: Nanostructured Materials for Engineering Applications. (Springer-Verlag, Berlin Heidelberg, 2011) pp. 23-140.
2. A.L. Barabási: Self assembled island formation in heteroepitaxial growth. *Appl. Phys. Lett.* **70,** 2565 (1997).
3. K. Reichelt, Nucleation and growth of thin films. *Vacuum* **38**, 1099 (1988).
4. J. Narayan, and B.C. Larson: Domain epitaxy: A unified paradigm for thin film growth. *J. Appl. Phys.* **93**, 278 (2003).
5. J. Tersoff, and F.K. LeGoues: Competing relaxation mechanisms in strained layers. *Phys. Rev. Lett.* **72**, 3570 (1994).
6. J. Nogami, B.Z. Liu, M.V. Katkov, C. Ohbuchi, and N.O. Birge: Self-assembled rare-earth silicide nanowires on Si(100). *Phys. Rev. B* **63**, 233305 (2001).
7. U. Gösele, and K.N. Tu: Growth kinetics of planar binary diffusion couples: “Thin-film case” versus “bulk cases”. *J. Appl. Phys.* **53**, 3252 (1982).
8. R. Anderson, J. Baglin, J. Dempsey, W. Hammer, F.d’Heurle, and S. Petersson: Nucleation-controlled thin-film interactions: Some silicides. *Appl. Phys. Lett.* **35**, 285 (1979).
9. F.M. d'Heurle: Nucleation of a new phase from the interaction of two adjacent phases: Some silicides. *J. Mater. Res.* **3**, 167 (1988).

10. F. Alharbi, J.D. Bass, A. Salhi, A. Alyamani, H.C. Kim, and R.D. Miller: Abundant non-toxic materials for thin film solar cells: Alternative to conventional materials. *Renew. Energ.* **36**, 2753 (2011).

11. Y. Makita, Y. Nakayama, Y. Fukuzawa, S.N. Wang, N. Otogawa, Y. Suzuki, Z.X. Liu, M. Osamura, T. Ootsuka, T. Mise, and H. Tanoue: Important research targets to be explored for β-$FeSi_2$ device making. *Thin Solid Films* **461**, 202 (2004).

12. Z. Liu, S. Wang, N. Otogawa, Y. Suzuki, M. Osamura, Y, Fukuzawa, T. Ootsuka, Y, Nakayama, H. Tanoue, and Y. Makita: A thin-film solar cell of high quality β-$FeSi_2$/Si heterojunction prepared by sputtering. *Sol. Energ. Mat. & Sol. Cell.* **90**, 276 (2006).

13. M. Shaban, K. Nakashima, W. Yokoyama, and T. Yoshitake: Photovoltaic properties of n-type β-$FeSi_2$/p-type Si heterojunctions. *Jap. J. Appl. Phys.* **46**, L667 (2007).

14. A.S.W. Wong, G.W. Ho, S.L. Liew, K.C. Chua, and D.Z. Chi: Probing the growth of β-$FeSi_2$ nanoparticles for photovoltaic applications: a combined imaging and spectroscopy study using transmission electron microscopy. *Prog. Photovolt: Res. Appl.* **19**, 464 (2011).

15. Y. Gao, H.W. Liu, Y. Lin, and G. Shao: Computational design of high efficiency $FeSi_2$ thin-film solar cells. *Thin Solid Films* **519**, 8490 (2011).

16. G.K. Dalapati, S.L. Liew, A.S.W. Wong, Y. Chai, S.Y. Chiam, and D.Z. Chi: Photovoltaic characteristics of p-β-$FeSi_2$(Al)/n-Si(100) heterojunction solar cells and the effects of interfacial engineering. *Appl. Phys. Lett.* **98**, 013507 (2011).

17. T. Buonassisi, A.A. Istratov, M.A. Marcus, B. Lai, Z. Cai, S.M. Heald, and E.R. Weber: Engineering metal-impurity nanodefects for low-cost solar cells. *Nature Materials* **4**, 676 (2005).

18. S. Terasawa, T. Inoue, and M. Ihara: Fabrication of β-$FeSi_2$/Si composite films for photovoltaic applications using scanning annealing. *Sol. Energ. Mater. & Sol. Cells* **93**, 215 (2009).

19. D.B. Migas, and L. Miglio: Band-gap modifications of β-$FeSi_2$ with lattice distortions corresponding to the epitaxial relationships on Si(111). *Phys. Rev. B* **62**, 11063 (2000).

20. K. Yamaguchi, and K. Mizushima: Luminescent $FeSi_2$ Crystal structures induced by heteroepitaxial stress on Si(111). *Phys. Rev. Lett.* **86**, 6006 (2001).

21. K.A. Mäder, H. von Känel, and A. Baldereschi: Electronic structure and bonding in epitaxially stabilized cubic iron silicides. *Phys. Rev. B* **48**, 4364 (1993).

22. H. von Känel, K.A. Mäder, E. Müller, N. Onda, and H. Sirringhaus: Structural and electronic properties of metastable epitaxial $FeSi_{1+x}$ films on Si(111). *Phys. Rev. B* **45**, 13807 (1992).

23. N. Jedrecy, A. Waldhauer, M. Sauvage-Simkin, R. Pinchaux, and Y. Zheng: Structural characterization of epitaxial α-derived $FeSi_2$ on Si(111). *Phys. Rev. B* **49**, 4725 (1994).

24. P. Villars, and L.D. Calvert: Pearson's Handbook of Crystallographic Data for Intermetallic Phases, Vol. 3, (American Society for Metals, Metals Park, OH, 1985), p. 2232.

25. G. Molnár, L. Dózsa, G. Pető, Z. Vértesy, A.A. Koós, Z.E. Horváth, and E. Zsoldos: Thickness dependent aggregation of Fe-silicide islands on Si substrate. *Thin Solid Films* **459**, 48 (2004).

26. C.A. Dimitriadis, and J.H. Werner: Growth mechanism and morphology of semiconducting $FeSi_2$ films. *J. Appl. Phys.* **68**, 93 (1990).

27. N. Vouroutzis, T.T. Zorba, C.A. Dimitriadis, K.M. Paraskevopoulos, L. Dózsa, and G. Molnár: Growth of β-$FeSi_2$ particles on silicon by reactive deposition epitaxy. *J. Alloys Compounds* **448**, 202 (2008).

28. M. Zinke-Allmang: Phase separation on solid surfaces: nucleation, coarsening and coalescence kinetics. *Thin Solid Films* **346**, 1 (1999).

29. S.Y. Chen, H.C. Chen, and L.J. Chen: Self–assembled endotaxial α-$FeSi_2$ nanowires with length tunability mediated by a thin nitride layer on (001)Si. *Appl. Phys. Lett.* **88**, 193114 (2006).

30. J.C. Mahato, D. Das, R.R. Juluri, R. Batabyal, A. Roy, P.V. Satyam, and B.N. Dev: Nanodot to nanowire: a strain-driven shape transition in self-organized endotaxial $CoSi_2$ on Si(100). *Appl. Phys. Lett.* **100**, 263117 (2012).

Journal of Materials Research 28 (13) 1724-1728 (2013)

Table I. The average number/μm^2, and average size of the nanostructures versus annealing temperature

Annealing temperature:	500°C	600°C	850°C
Number of objects:	330/μm^2	65/μm^2	30/μm^2
Average size of objects:	20 nm	80 nm	100 nm

Journal of Materials Research 28 (13) 1724-1728 (2013)

Figure captions

Fig. 1 RHEED images of (a) the cleaned and annealed Si(001) substrate, showing 2x1 reconstruction, which indicates the high quality of the surface. RHEED images of evaporated 1 nm Fe layer after annealing for 60 minutes on Si(001) at (b) 500ºC (c) 600°C, and (d) 850°C for iron silicide formation. The images show the epitaxial character of the formed iron silicide but, the weak and diffuse lines refer to a moderate quality surface.

Fig. 2 SEM images of 1.0 nm iron annealed on Si(001) for 60 min at (a) 500°C, (b) 600°C, (c) 850°C.

Fig. 3 SEM images of 1.0 nm iron annealed at 600°C for 60 min at enhancing ((a) towards (c)) magnifications. The circular objects show the nucleation controlled growth of iron silicide at nanoscale.

Fig. 4 Optical microscopy image of thin film type (30 nm evaporated Fe annealed at 600°C for 5 min) iron silicide sample showing typical nucleation controlled growth.

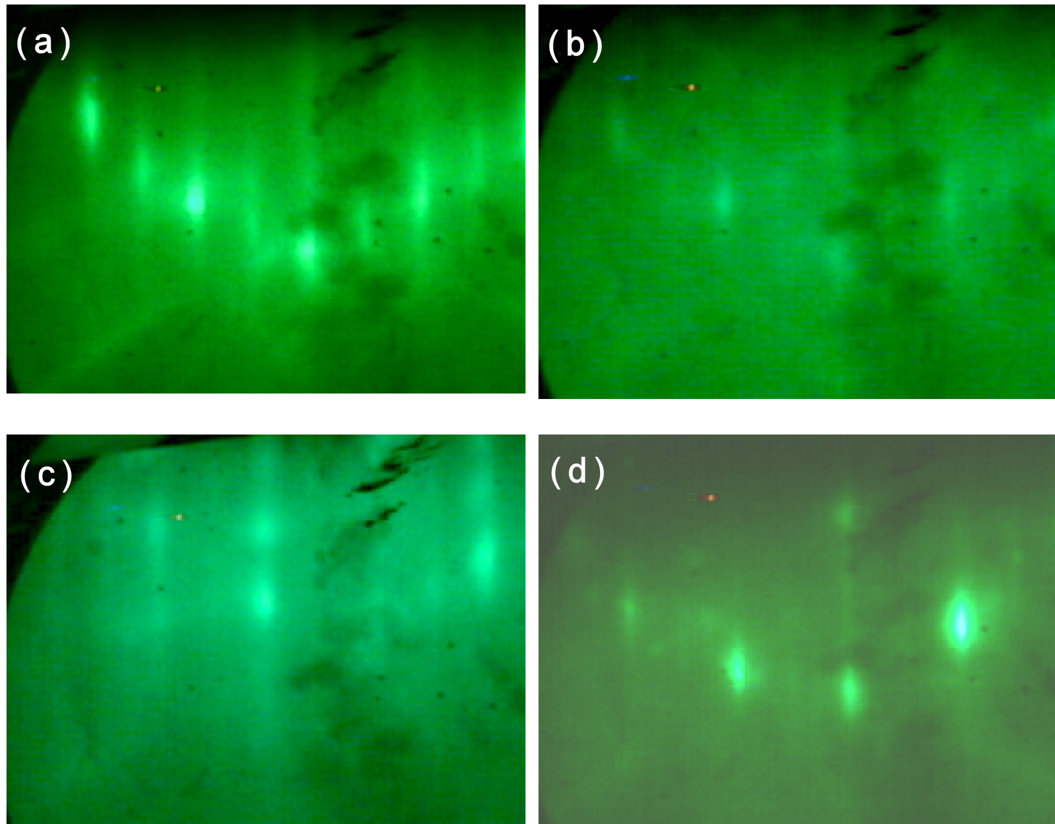

Fig. 1 *RHEED images of (a) the cleaned and annealed Si(001) substrate, showing 2x1 reconstruction, which indicates the high quality of the surface. RHEED images of evaporated 1 nm Fe layer after annealing for 60 minutes on Si(001) at (b) 500ºC (c) 600°C, and (d) 850°C for iron silicide formation. The images show the epitaxial character of the formed iron silicide but, the weak and diffuse lines refer to a moderate quality surface.*

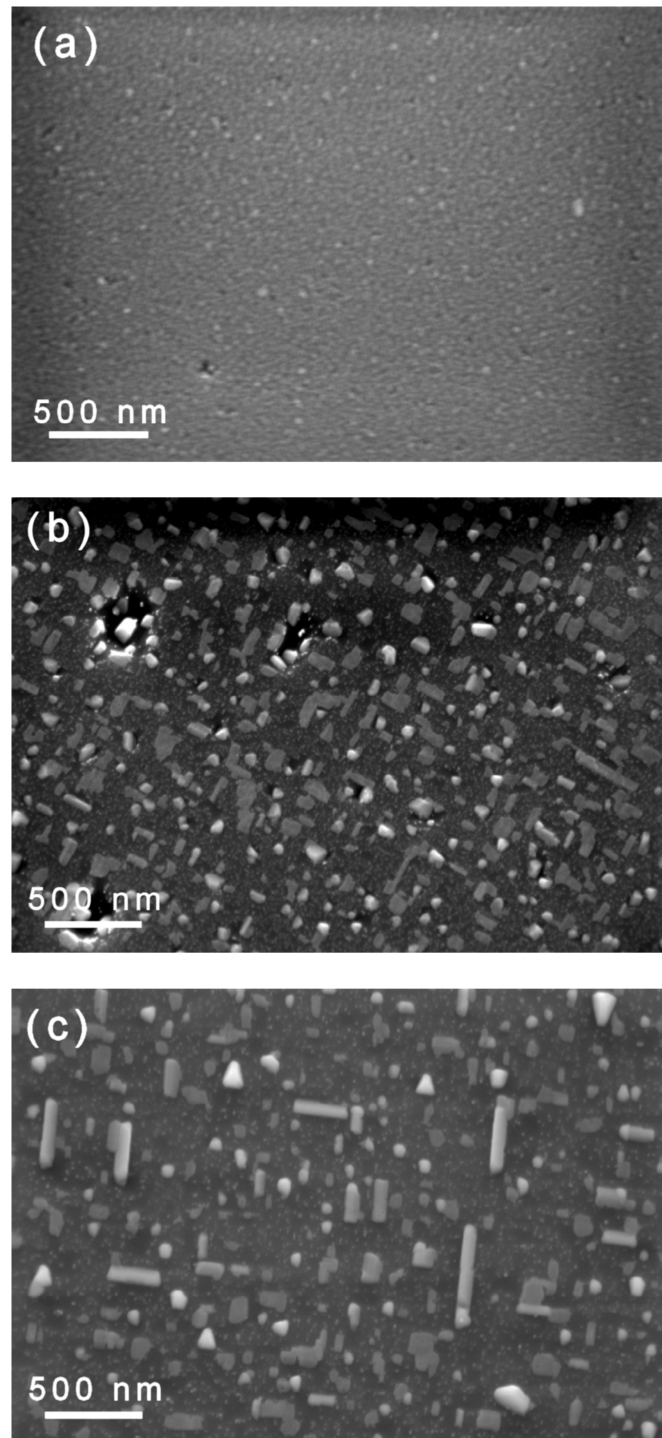

Fig. 2 SEM images of 1.0 nm iron annealed on Si(001) for 60 min at (a) 500°C, (b) 600°C, (c) 850°C.

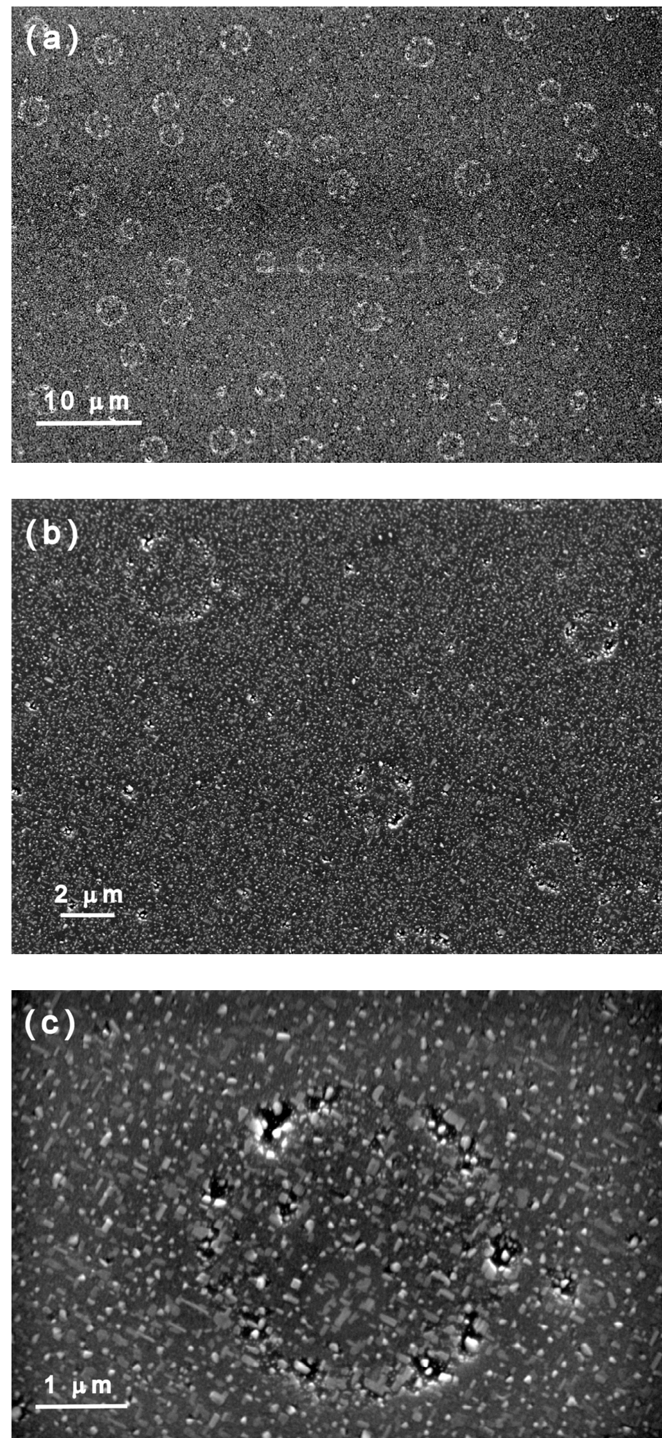

Fig. 3 *SEM images of 1.0 nm iron annealed at 600°C for 60 min at enhancing ((a) towards (c)) magnifications. The circular objects show the nucleation controlled growth of iron silicide at nanoscale.*

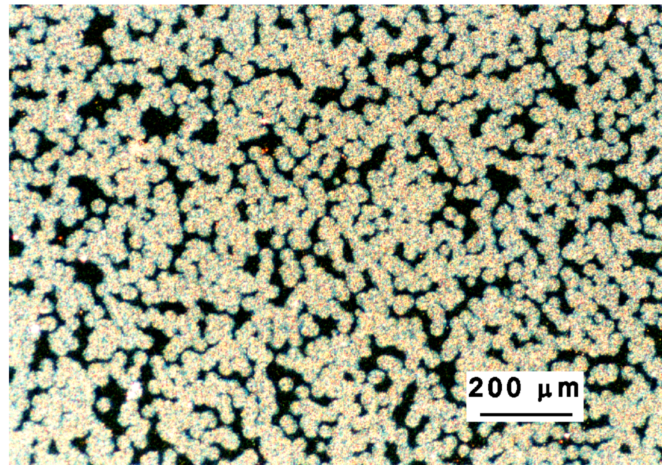

Fig. 4 Optical microscopy image of thin film type (30 nm evaporated Fe annealed at 600°C for 5 min) iron silicide sample showing typical nucleation controlled growth.